AD-A261 197

Research and Development Technical Report
SLCET-TR-91-18

# Use of Permanent Magnets in Magnetron Design


Anup S. Tilak, Herbert A. Leupold and
Ernest Potenziani II
Electronics Technology and Devices Laboratory


July 1991



DISTRIBUTION STATEMENT
Approved for public release.
Distribution is unlimited.




U. S. ARMY LABORATORY COMMAND
Electronics Technology and Devices Laboratory
Fort Monmouth, NJ 07703-5601

# NOTICES

## Disclaimers

# REPORT DOCUMENTATION PAGE

*Form Approved*
*OMB No. 0704-0188*



**1. AGENCY USE ONLY** *(Leave blank)*

**2. REPORT DATE**
July 1991

**3. REPORT TYPE AND DATES COVERED**
Technical Report: 1990-1991

**4. TITLE AND SUBTITLE**
USE OF PERMANENT MAGNETS IN MAGNETRON DESIGN

**5. FUNDING NUMBERS**
PE: 060110
PR: 1L161102AH47
TA: 01
WU: 04 DA302913

**6. AUTHOR(S)**
Anup S. Tilak, Herbert A. Leupold and Ernest Potenziani II

**7. PERFORMING ORGANIZATION NAME(S) AND ADDRESS(ES)**
US Army Laboratory Command (LABCOM)
Electronics Technology and Devices Laboratory (ETDL)
ATTN: SLCET-EA
Fort Monmouth, NJ 07703-5601

**8. PERFORMING ORGANIZATION REPORT NUMBER**
SLCET-TR-91-18

**9. SPONSORING/MONITORING AGENCY NAME(S) AND ADDRESS(ES)**

**10. SPONSORING/MONITORING AGENCY REPORT NUMBER**

**11. SUPPLEMENTARY NOTES**

**12a. DISTRIBUTION/AVAILABILITY STATEMENT**
Approved for public release; distribution is unlimited.

**12b. DISTRIBUTION CODE**

**13. ABSTRACT** *(Maximum 200 words)*
Several alternative designs for a magnetron/gyrotron, permanent-magnet solenoid are analyzed with regard to magnetic field uniformity and magnitude, structural weight, susceptibility to heating, and access hole size. Structural masses were found to range from about 10 kilograms to 60 kilograms depending on details of design and or the type of permanent magnet tube. Recommendations are made as to the best choices for the intended purpose.

**14. SUBJECT TERMS**
Permanent-magnet solenoids; magnetrons; gyrotrons; magnetic cladding; azimuthal dependence of field

**15. NUMBER OF PAGES**
30

**16. PRICE CODE**

| 17. SECURITY CLASSIFICATION OF REPORT | 18. SECURITY CLASSIFICATION OF THIS PAGE | 19. SECURITY CLASSIFICATION OF ABSTRACT | 20. LIMITATION OF ABSTRACT |
|---|---|---|---|
| Unclassified | Unclassified | Unclassified | UL |

# Table of Contents

## List of Figures

# USE OF PERMANENT MAGNETS IN MAGNETRON DESIGN

## INTRODUCTION

All magnetrons require a cathode and an anode with a dc magnetic field perpendicular to the dc electric field between them. The electrons emitted by the cathode are influenced by the crossfields to move in curved paths in the interaction region. They continue to drift towards the positively polarized anode where they are ultimately collected.

This study deals with the feasibility of permanent magnet field sources in magnetrons. A dc magnetic field of about 7.5 kOe ±5% was required in an interaction region that is 7.2 cm long and 0.53 cm wide. Several suitable options were investigated and are compared in this report.

## DESIGN SPECIFICATIONS

Figure 1 shows the longitudinal cross section of the magnetron that was the subject of this investigation and Figure 2 shows its transverse cross section. As indicated in Figure 2, the outer radius of the cathode $R_1$ is 1.58 cm and the inner radius of the anode, $R_2$, is 2.11 cm. The interaction region, between the anode and the cathode, is 0.53 cm across; and the outer radius of the anode block, $R_4$, is 4.62 cm. The cavity angles in the anode block are 20° and two of the cavities, diametrically across from one another, serve as entry ports for the waveguides needed for the rf output. The waveguide extends 7.0 cm along the 7.2 cm length of the structure. The dc electric field and the magnetic field are respectively perpendicular and parallel to the structural axis.

## THEORY

Details of a clad cylindrical longitudinal field structure have been described elsewhere.[1-3] Provisions for a field $H_W$ = 7.5 kOe in a cylindrical space of radius 4.62 cm and length 7.20 cm requires a flux $\Phi_W$ in the interaction region of

$$\Phi_W = \pi R_4^2 H_W = 503 \text{ kMx} \tag{1}$$

This flux is to be supplied by a longitudinally oriented magnet encompassing the working space as shown in Figure 3. Hence,

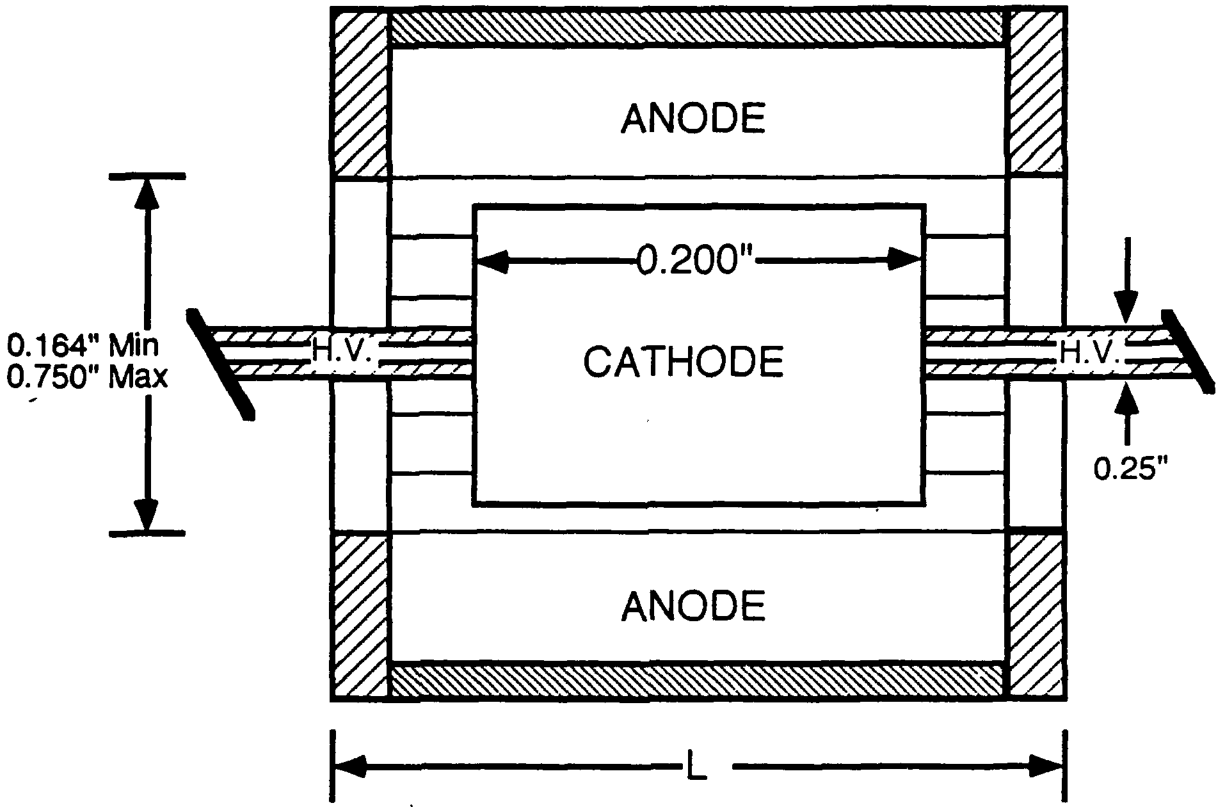


Figure 1. Longitudinal cross section of magnetron.

$$A_M B_M = 503 \text{ kMx} \tag{2}$$

where $A_M$ is the cross-sectional area of the supply magnet and $B_M$ is given by

$$B_M = B_R - H_W \tag{3}$$

where $B_R$ is the remanence of the magnetic material used, so

$$A_M = 112 \text{ cm}^2 \tag{4}$$

To keep the flux confined to the space within $R_4$ we need a tapered, radially oriented, cladding magnet encasing the longitudinal supply magnet as shown in Figure 4. The maximum thickness $t_r$ of the former magnet is given by reference 2 as

$$t_r = H_W L_W / 2B_R = 2.25 \text{ cm} \tag{5}$$

where $L_W$ is the length of the working space.

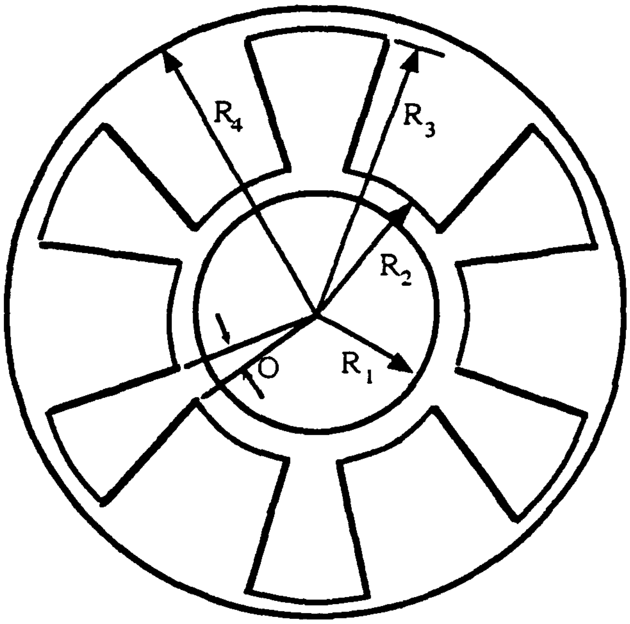


| | | |
|---|---|---|
| $R_1$ Cathode O.R. | 1.58 cm | 0.62 inch |
| $R_2$ Anode I.R. | 2.11 cm | 0.82 inch |
| $R_3$ Anode O.R. | 4.11 cm | 1.62 inch |
| $R_4$ Anode Block O.R. | 4.62 cm | 1.82 inch |
| O Cavity Angle | 20 degrees | |
| L Circuit Length | 7.20 cm | 2.83 inches |

Figure 2. Transverse cross section of magnetron.

To prevent end losses, we must have disc-shaped bucking magnets, pole pieces and tapered ring-shaped corner magnets as shown in Figure 4. The bucking magnets must have a thickness equal to $t_r$ of the radial annular magnet, namely 2.25 cm. The pole pieces must be of sufficient thickness to carry 503 kMx of flux. If iron is used with a saturation induction of 20 kG, the circumferential area $A_p$ of each disc is given by

$$A_p = 503 \text{ kMx}/20 \text{ kG} = 25.2 \text{ cm}^2 \tag{6}$$

so that the thickness of the pole piece must be at least

$$t_p = A_p/2\pi R_4 = 0.866 \text{ cm} \tag{7}$$

(a)

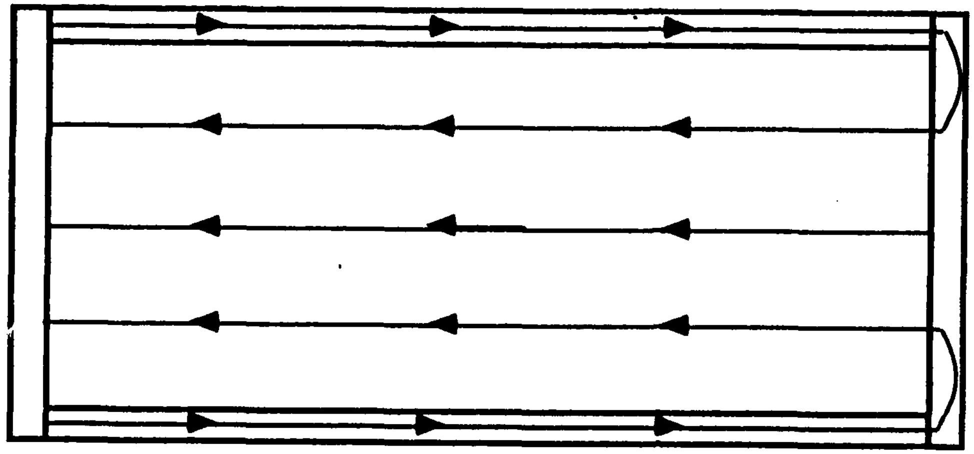

$$H_M = H_W$$

$$B_M A_M = H_W A_W$$

$$B_M = \mu H_M + B_A$$

$$A_M = A_W / (\mu_A - B_A / H_W) \quad \text{for } H_W < 0$$

(b)

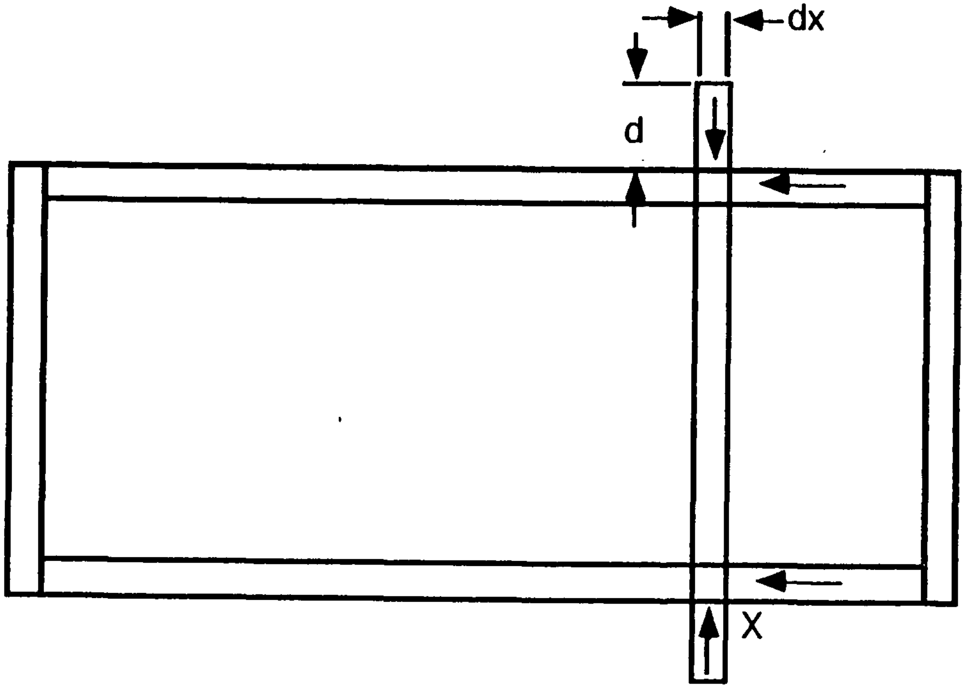


$$H_C d = H_M x$$

$$d = H_W x / H_C$$

Figure 3. (a) Determination of supply magnet cross-section.
(b) Determination of cladding thickness.

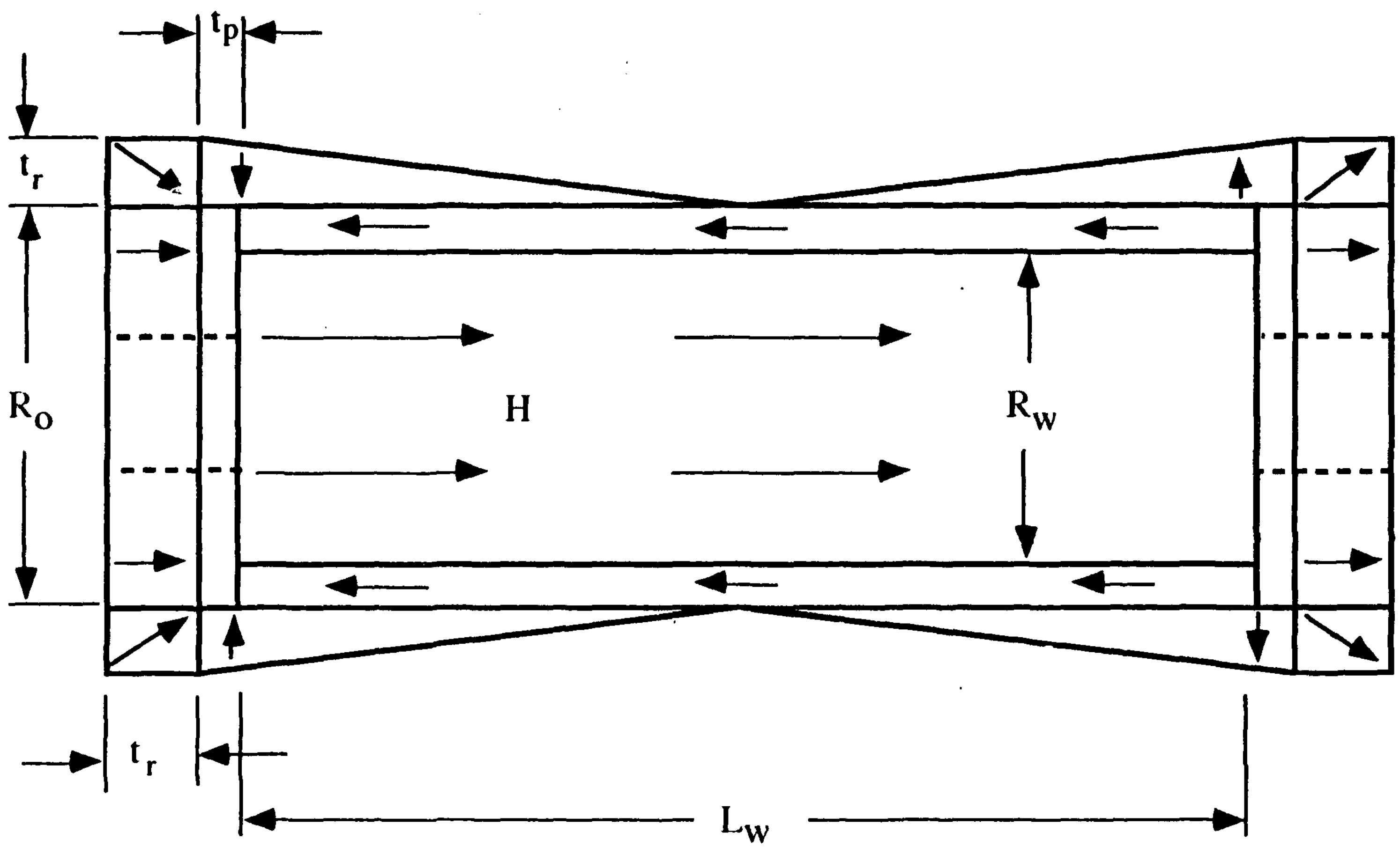


Figure 4. Design for a traditional symmetrically cladded constant field permanent magnet solenoid.

## PRELIMINARY INVESTIGATION: POSSIBLE CONFIGURATIONS

Figure 5 shows the three possibilities investigated.

A. IDEAL CASE: A magnetic material of $B_R = 12$ kG is used for all magnets and all of the supply magnet, 41.9 $cm^2$ is placed in the interior of the tube. Part of the magnet material, 7.84 $cm^2$, is placed in the central core within the cathode and the remainder, 34.1 $cm^2$, is placed in the space available within the anode block. The total mass of this structure, when permanent magnets with $\rho = 7.7$ g/$cm^3$ are used, is approximately 11.3 kg. A 2-D finite element plot of the structure is shown in Figure 6. As can be seen, the field uniformity over the entire region of the structure is very good. Figure 7 shows the field profile along the length of the interaction region. The field is 6.5 kOe over most of the range with a 5.6% decline towards the edges of the tube. The 7% leakage due to imperfect cladding accounts for the 6.5 kOe peak field in a configuration designed to yield a 7.0 kOe field. Entry ports for the wave guide require that part of the cladding be removed. This adds to the leakage of flux and results in further reduction in peak magnetic field.

This ideal configuration yields a very compact low-mass device. However, it uses all the available space within the magnetron tube, leaving no room for cooling systems which are necessary for effective heat transfer. Without such transfer, the magnet warms up to a high temperature which results in a decrease in magnet remanence and hence magnetic field. Moreover, the commercial availability of magnetic materials of remanence 12 kG is suspect.

B. WORST CASE: Magnetic material of $B_R = 11.5$ kG is used for all magnets and all of the supply magnet is placed exterior to the tube and the model is designed for a peak field of 7.5 kOe. External placement of the magnetic material affords ready cooling. The dimensions of the structure were determined by a process similar to the one described earlier and it yields

supply magnet thickness = 3.21 cm
maximum cladding thickness = 2.38 cm
thickness of pole piece = 0.511 cm
mass of magnetic structure = 23.9 kg
for magnetic materials of density $\rho = 7.7$ g/$cm^3$

A 2D-finite element plot of the structure is shown in Figure 8 and the field uniformity over the entire region of the structure is remarkable. Figure 9 shows the field profile along the length of the structure. The field is 7.0 kOe for most of the circuit length with a 0.54% decline towards the edges of the tube. The leakage is about 7%.

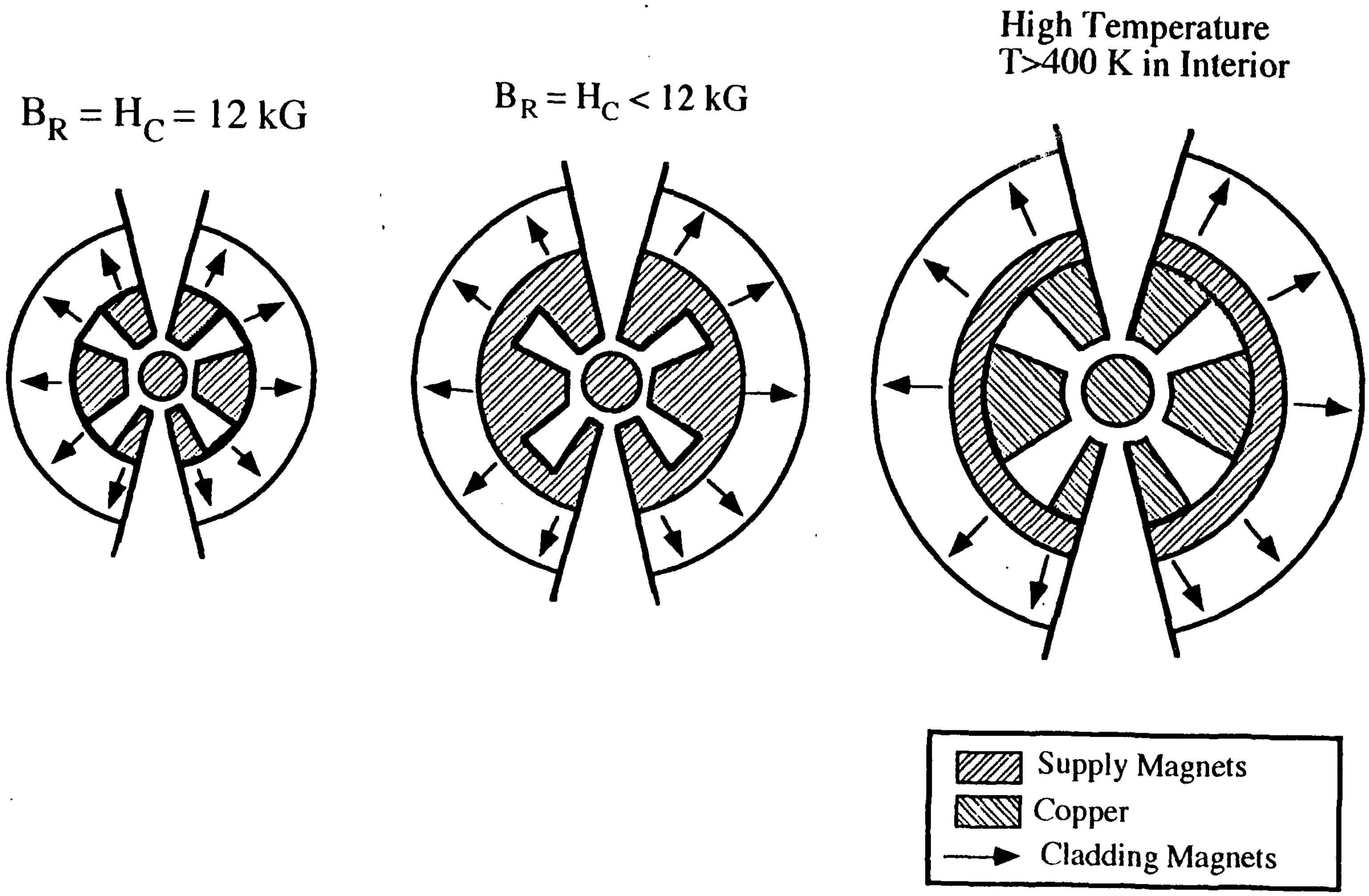


Figure 5. Three alternatives for permanent magne. placement in magnetron.

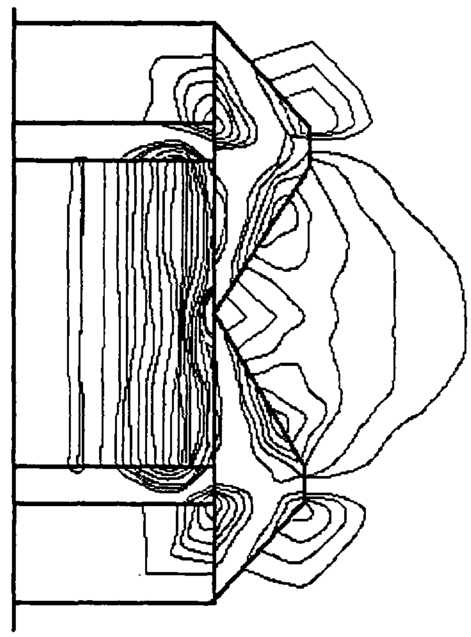

Figure 6. A 2-D finite element plot for the ideal case design.

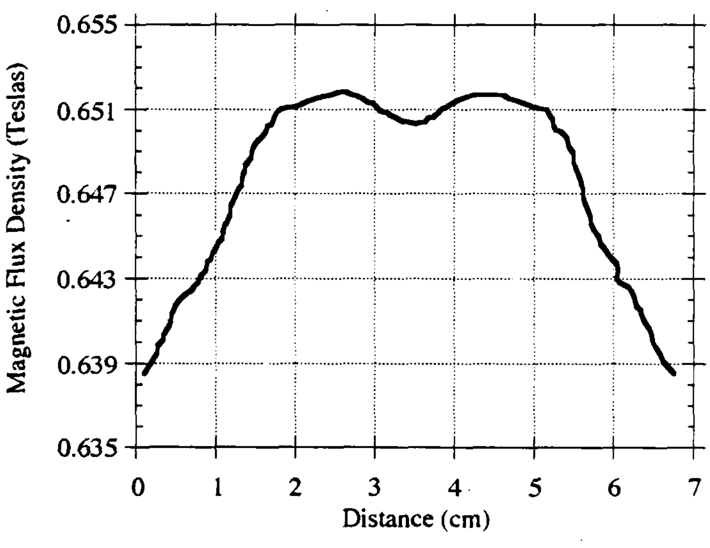


Figure 7. Field profile in the interaction region of the ideal design.

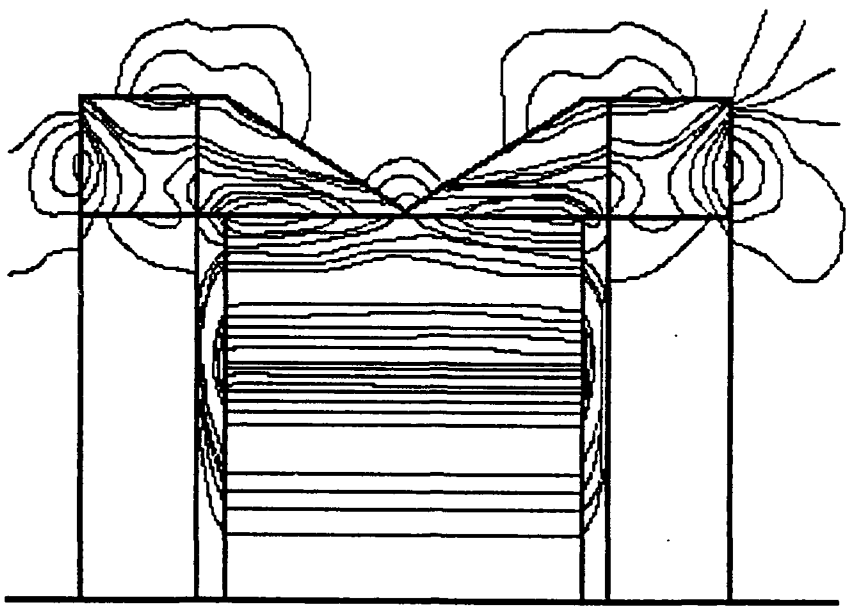

Figure 8. A 2-D finite element plot for the worst case design.

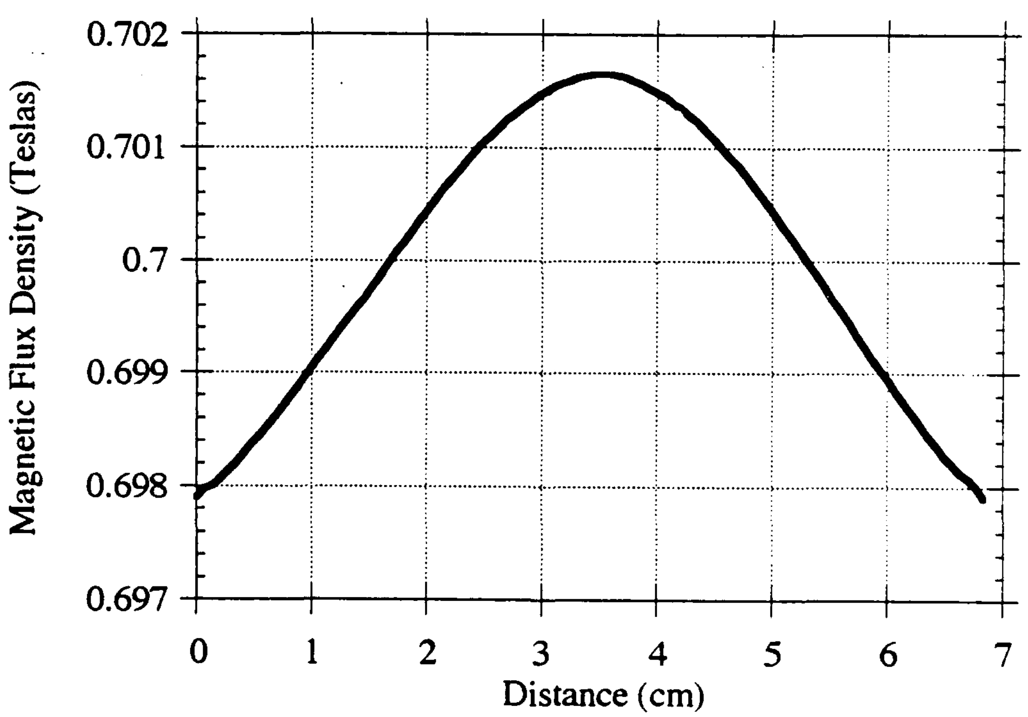


Figure 9. Field profile in the interaction region of the worst case design.

This worst case scenario yields a device that is more massive but free of complications arising from magnetic material deterioration due to heating. Adequate room exists for strategic placement of cooling systems which will ensure good magnetic field quality during operation. As in the ideal case, part of the cladding magnet has to be removed to allow for insertion of waveguides. The flux leakage at the insertion site is unavoidable. Also, this configuration demands that part of the supply magnet be removed as well. As long as the portion of the removed supply magnet is included elsewhere in the arrangement, it is rather forgiving as far as placement site is concerned. It does, however, push the cladding further out, resulting in an additional increase in mass.

C. INTERMEDIATE CASE: A theoretical assessment was also made for an intermediate arrangement, shown in Figure 10. Part of the magnetic material is placed within the magnetron tube inside the cathode, and the remainder outside the anode block. For a magnetic material of remanence $B_R = 11$ kG and $\rho$=7.7 g/cm$^3$, the expected mass of this configuration would be 13 kg. The smaller $B_R$ chosen for this case reflects the probability of greater heating due to closer proximity of magnetic material to the interaction region, as the required temperature stability is available only in materials with a $B_R$ of less than 11 kG.

The results of the three possibilities analyzed in the preliminary investigation are summarized in the table presented in Figure 11.

## EFFECT OF WAVEGUIDE PORTS ON FIELD UNIFORMITY

An exact treatment of field irregularities resulting from missing cladding at the waveguide portals of the ideal structure was made when a computer program for three dimensional analysis became available. Originally, an estimate of the magnitude of the effect was gleaned from a computation of the field contribution $H_S$ of the side cladding taken together with the pole pieces. The field contribution of the missing cladding $H_M$ everywhere in the interaction region was then found to be of the order of

$$H_M \approx (40/360)H_S = H_S/9$$

The variation of $H_M$ around the circumference of the interaction region $\Delta H_M$ is very much smaller than $H_M$ itself so that

$$\Delta H_M << H_M = H_S/9$$

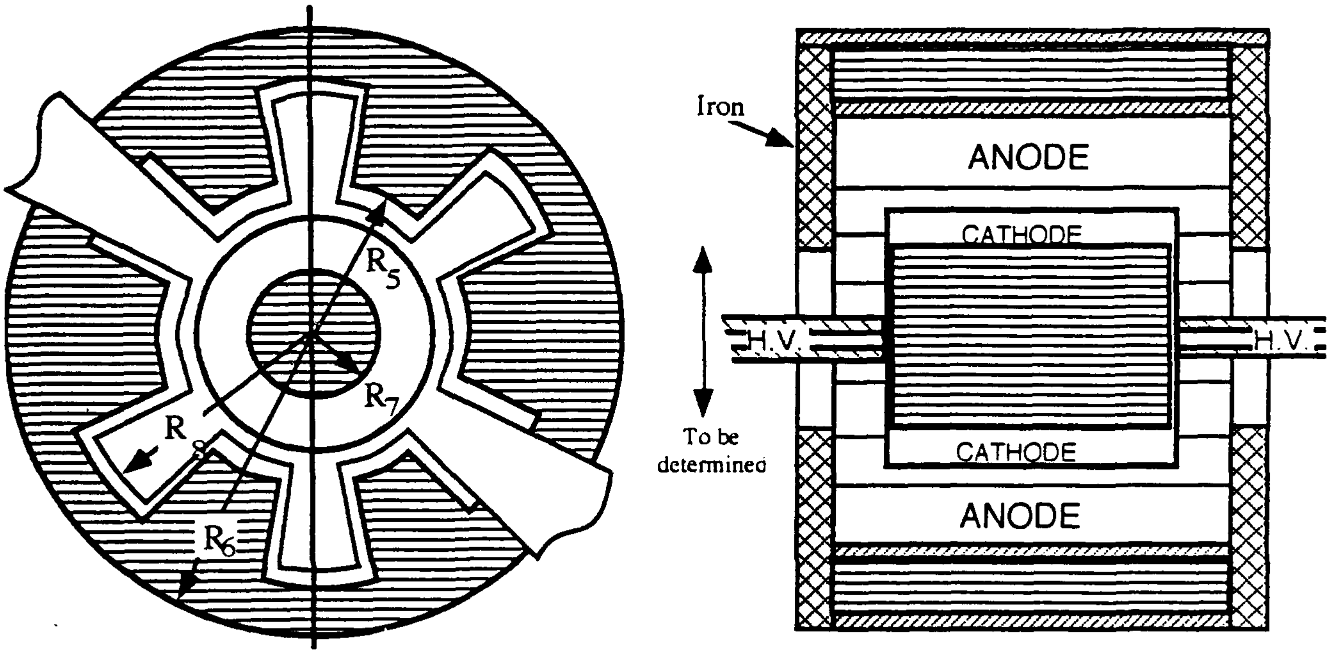


DIMENSIONS

| | |
|---|---|
| $R_5$ - Magnetic Material Inner Radius | 2.60 cm (1.02 in) |
| $R_6$ - Magnetic Material Outer Radius | To be determined |
| $R_7$ - Cathode Region Magnet Outer Radius | 1.27 cm (0.5 in) |
| $R_8$ - 2nd Magnetic Material Inner Radius | 4.11 cm (1.62 in) |

* Note: $R_5$ and 0.100 Dim allow for possible cooling channels

Figure 10. Magnet location in the intermediate choice.

and since $H_S$ is only one percent of the total field, the effect of $H_M$ is expected to be negligible. The three-dimensional analysis confirmed this conclusion as it showed an azimuthal field variation of only a few parts per thousand as is shown in the plot of Figure 13. More details of the analysis are given in the appendix.

| No. | Scenario | Description | Mass | Leakage | Variation |
|---|---|---|---|---|---|
| 1 | Ideal Case | Magnet of Remanence = 12 kG<br>All in the tube interior | 11.5 kg | 7% | 6900 - 7000 G |
| 2 | Worst Case | Magnet of Remanence = 11.5 kG<br>All exterior to tube | 23.85 kg | 7% | 6980 - 7000 G |
| 3 | Intermediate Case | Magnet of Remanence = 11 kG<br>Partially exterior to tube | | | |

Figure 11. Magnet mass and magnetic field summary for the three choices.

## FINAL ANALYSIS

In the final analysis, it was determined that in view of the quality of commercially available magnetic materials and the need to effectively remove the heat generated within the tube, all the magnet material be placed in a traditional configuration outside the anode block. Easily available permanent magnet materials of remanences BR = 10 kG and density = 7.7 g/cm$^3$ were used in the analysis. A structure was designed for a theoretical 7.0 kOe field in the interaction region. The mass of this configuration was considerably higher, 25.7 kg. The 2-D finite element plot of Figure 12 shows the field uniformity to be very good in the interaction region. Figure 13 shows that the field along the length of that region is about 6.0 kOe and is uniform to about 0.29%, indicating a flux leakage of approximately 7%, again because of imperfect cladding.

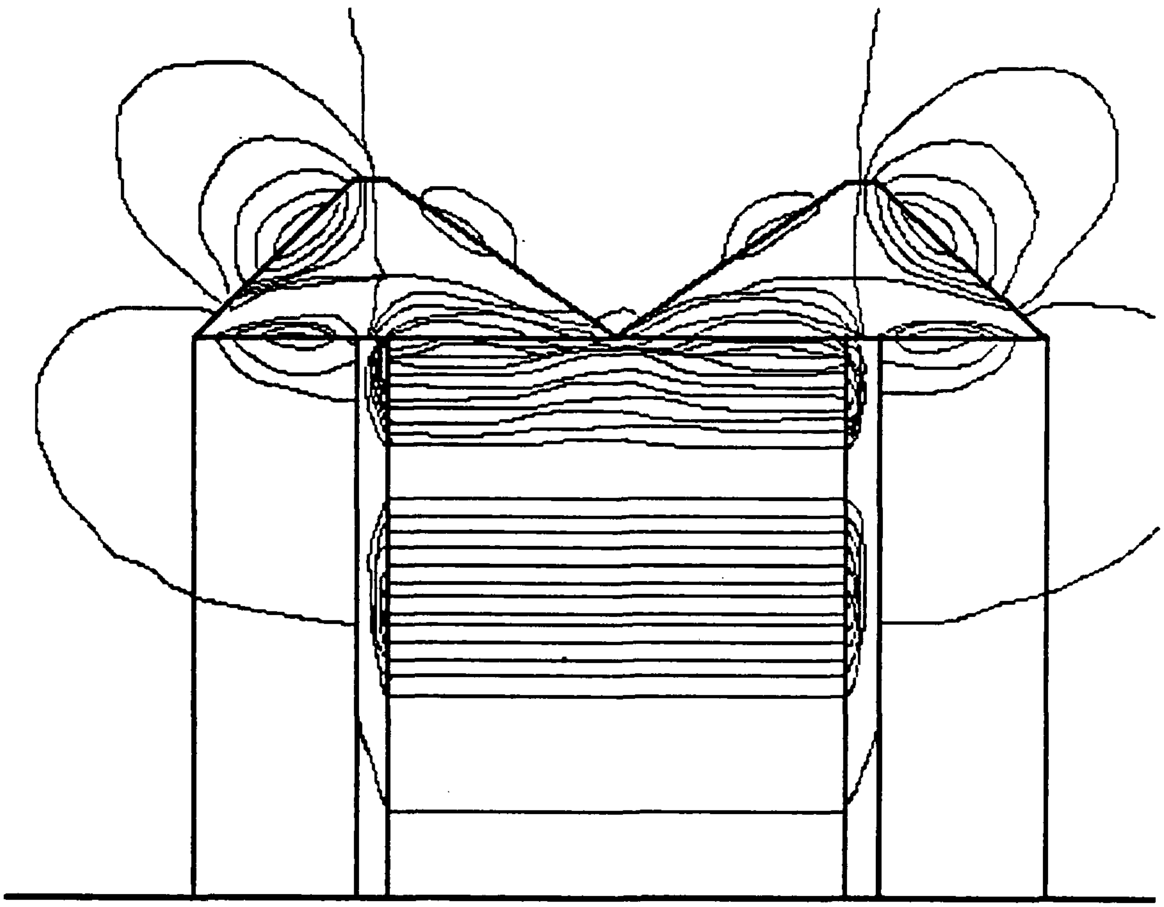

Figure 12. A 2-D finite element plot for the most practical design. Here the usual corner magnets of rectangular cross-section have been replaced by the equally effective and simpler radially oriented magnets of triangular cross-section.

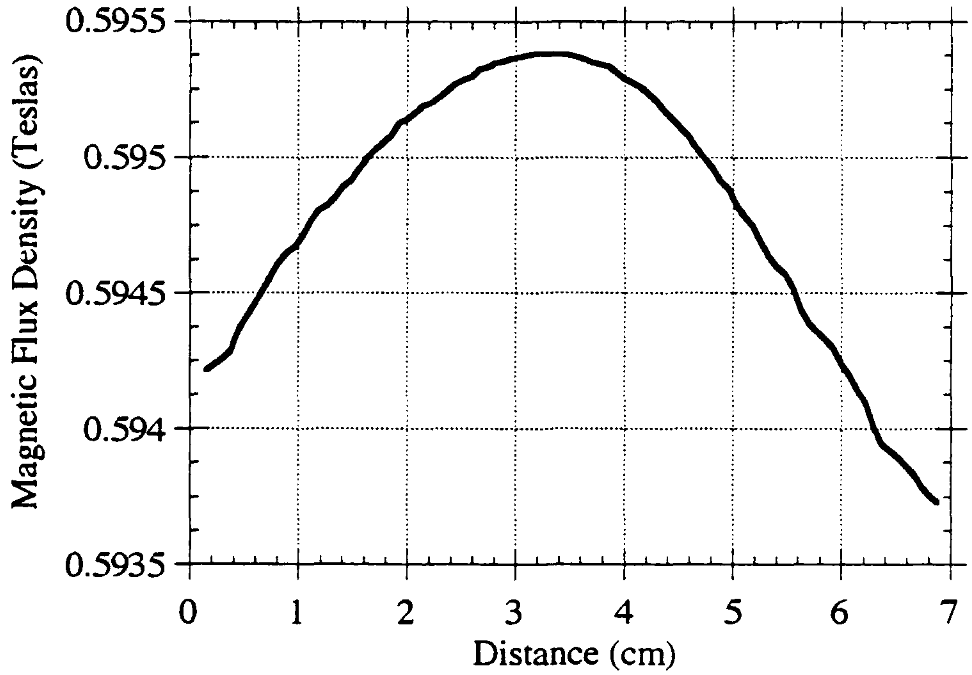


Figure 13. Field profile in the interaction region of the best choice.

Further modifications were then introduced as dictated by the electronics of the tube. To serve as possible entry and exit ports for electronic and thermal gadgetry, tunnels of varying diameter drilled at both ends of the above permanent magnet device were considered in the analysis. Figure 14 tabulates the peak fields and the field gradient along the length of the interaction region for a variety of models considered. Figure 15 shows the variation in peak field as a function of tunnel radius, a major factor in evaluating the possibilities before a judgment can be made with regard to a choice in hole diameter.

The possibility of increasing the tube length to 9.2 cm was also investigated. Although this would further add to the mass of the device, it would ensure field uniformity over the entire region of the rf output where the waveguides are inserted. The results are included in Figures 14 and 15.

## CONCLUSIONS

A prototype of the 7.2 cm long permanent magnet described above is under consideration. Magnetic materials such as $Sm_2Co_{17}$ ($\rho$ = 8.3 g/cm$^3$) and Nd-Fe-B ($\rho$ = 7.4 g/cm$^3$) are possible choices. The remanences of commercially available materials and their sensitivities to high temperatures would determine the final choice. The 7.0% leakage encountered throughout the investigation can be eliminated easily by a slight modification of the cladding as described in references 1 and 2.

| No. | Filename and Mass kg | Desired Field kOe | Magnet remanence kG | Bore Radius cm | On-axis Field (G) max | On-axis Field (G) min | On-axis Field (G) delta | Air gap Field (G) max | Air gap Field (G) min | Air gap Field (G) delta | Field across Work Space Oe |
|---|---|---|---|---|---|---|---|---|---|---|---|
| 1 | MM4 25.75 | 7 | 10 | 0 | 5952 | 5937 | .25% | 5954 | 5937 | .29% | 5962-5952 |
| 2 | MM8 25.75 | 7 | 10 | .3475 | 5928 | | | 5952 | 5940 | .20% | 5961-5948 |
| 3 | MM12 25.25 | 7 | 10 | .4166 | 5923 | | | 5950 | 5942 | .13% | 5961-5945 |
| 4 | MM9 25.75 | 7 | 10 | .5 | 5916 | | | 5947 | 5940 | .12% | 5960-5940 |
| 5 | MM10 25.75 | 7 | 10 | 1 | 5831 | | | 5906 | 5888 | .31% | 5950-5864 |
| 6 | MM13 25.25 | 7 | 10 | 1.5 | 5650 | | | 5788 | 5750 | .66% | 5933-5686 |
| 7 | MM11 25.25 | 7 | 10 | 1.905 | 5418 | | | 5670 | 5490 | 3.3% | 5910-5447 |
| 8 | MMX1 37.96 | 7 | 10 | 0 | 5900 | 5873 | .46% | 5904 | 5870 | .6% | 5927-5900 |
| 9 | MMX2 37.96 | 7 | 10 | .4166 | 5878 | | | 5900 | 5874 | .46% | 5924-5895 |
| 10 | MMX3 37.96 | 7 | 10 | 1 | 5823 | | | 5866 | 5838 | .45% | 5910-5851 |
| 11 | MMX4 37.96 | 7 | 10 | 1.905 | 5572 | | | 5737 | 5456 | 5.2% | 5853-5602 |

Figure 14. Permanent magnet choices for magnetrons: A summary.

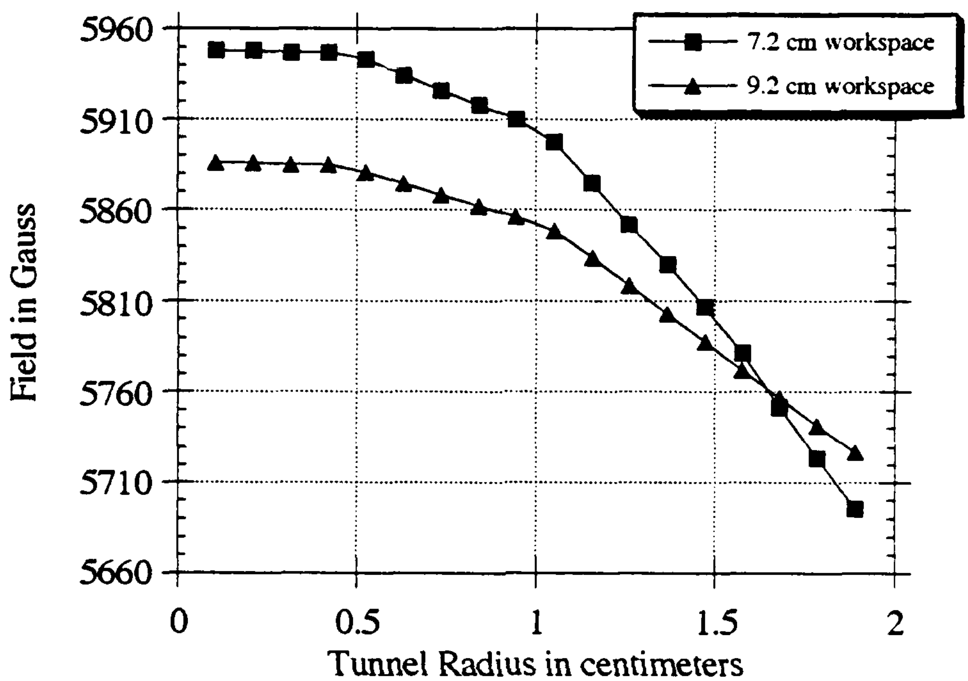


Figure 15. Peak field at electron orbit site as a function of the tunnel radius.

## REFERENCES


1. H. A. Leupold, E. Potenziani II, D. J. Basarab and A. S. Tilak, "*Magnetic field source for bichambered electron-beam devices*", J. Appl. Phys. 67(9), (1990)

2. E. Potenziani II and H. A. Leupold, IEEE Trans. Magn., **MAG-22**(5), 1078(1986)

3. J. P. Clark and H. A. Leupold, IEEE Trans. Magn., **MAG-22**(5), 1063(1986)

## APPENDIX A • Three-Dimensional Analysis

A three dimensional finite element analysis (FEM) was performed on the structure illustrated in Figure A-1. Figures A-2 thru A-5 show several cross-sectional cuts through the structure perpendicular to the axis of rotation. The various magnet orientations are shown by heavy arrows and all magnets were assumed to have a remanence of 10 kG (795,774 amps/meter).

Because computer disk and RAM requirements quickly grow to unmanageable proportions as problem complexity increases, we have used symmetry arguments to greatly simplify this analysis. Only one-half the length of the structure in the z-direction is modeled and this end "surface" is left unconstrained. Also, only 180° of the structure in the azimuthal direction is modeled. The resulting flat "surface" in this case is constrained to $A_x=A_z=0$ (where $\vec{A}$ is the vector potential). The slot for the waveguide extends from 80° to 100° in the azimuthal direction (by symmetry, there exists an identical waveguide slot in the opposite half of the structure that extends from 260° to 280°). A center hole size of 0.5 cm diameter was chosen for this analysis.

Figure A-6 is an overall view of the structure and Figure A-7 is the resulting FEM mesh. The structure is tilted down 25° about the x-axis and bulges outwards towards the reader.

The z-component of the magnetic field was plotted for several different paths, as shown in Figures A-8 thru A-10. In Figure A-8, $H_z$ is plotted, as one travels along the central axis of the structure, for several different radii. The point z=0 corresponds to the lowest point in the "air" working space, i.e., adjacent to the pole piece. For r=2 cm from the central axis, the field is relatively uniform along the length of the structure (the z-distance of 3.5 cm corresponds approximately to the midpoint of the structure along its length). For r=0.35 cm, the influence of the central hole (of radius 0.25 cm) is pronounced only a centimeter or less from the pole pieces.

Figures A-9 and A-10 are plots of $H_z$ along 180° arcs of r=2.1 cm and r=4.5 cm from the central axis. The horizontal axis corresponds to distance **along** each arc. The influence of the waveguide slit (at 80° to 100°) can be seen as a small decrease in field component in the middle third of each arc.

Overall, the variation in field in the entire working space is on the order of a few percent, but if one keeps to a particular path with a high degree of symmetry (e.g., an electron beam in a circular orbit around the central axis), a variation on the order of a few tenths of a percent can be realized. A detailed printout of all fields and related parameters is included.

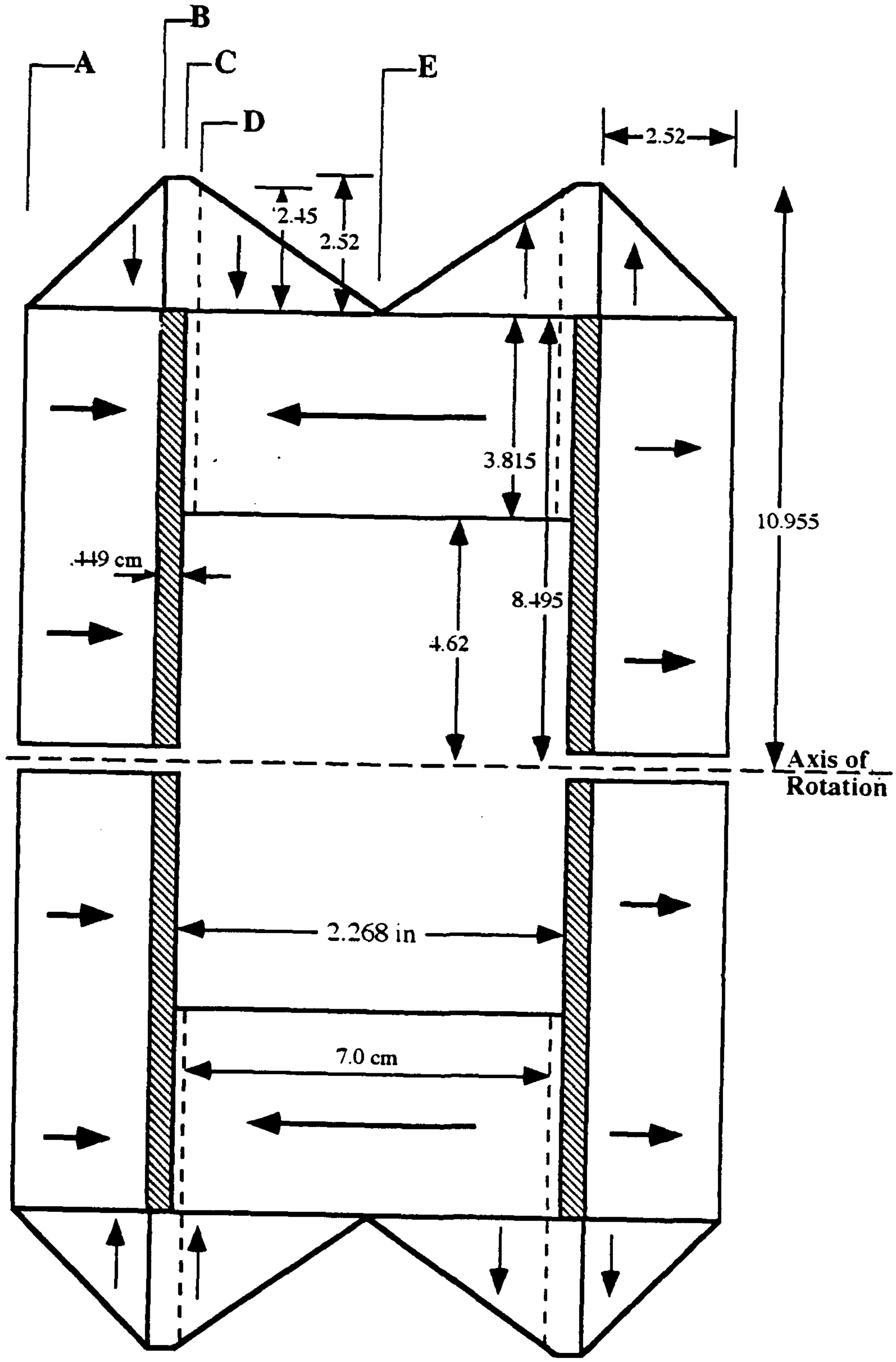


Figure A-1. Side view of the overall structure as used in the three-dimensional analysis. Overall length is 13.126 cm.

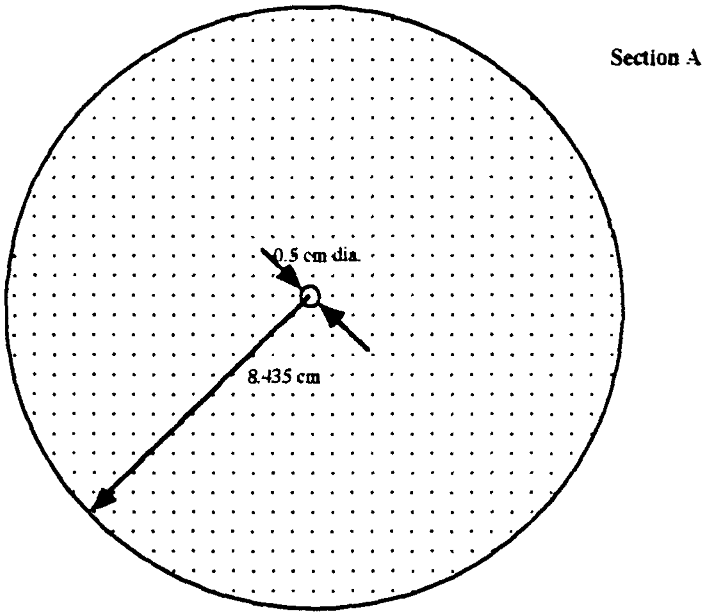


Figure A-2. View of cut through section A of figure A-1.

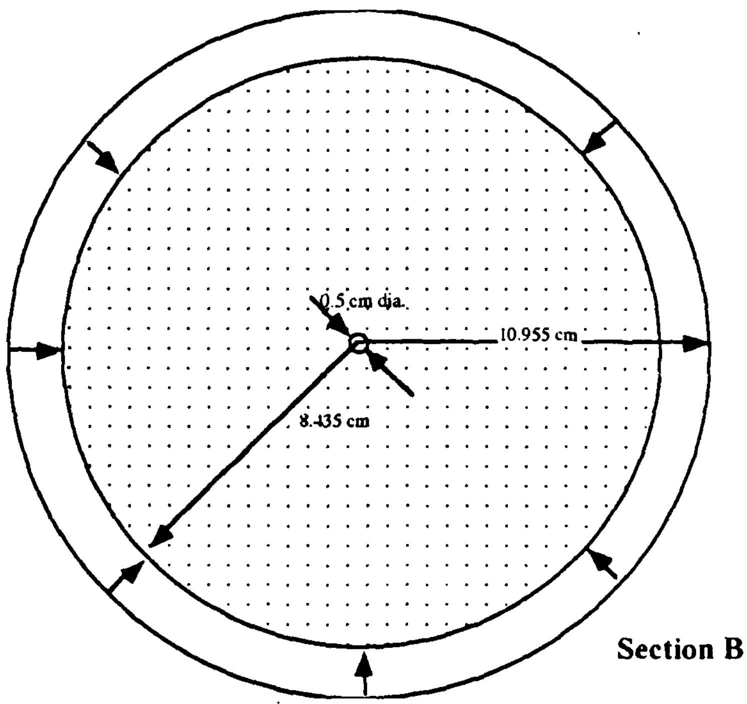


Figure A-3. Diagram of a cut through section B of figure A-1.

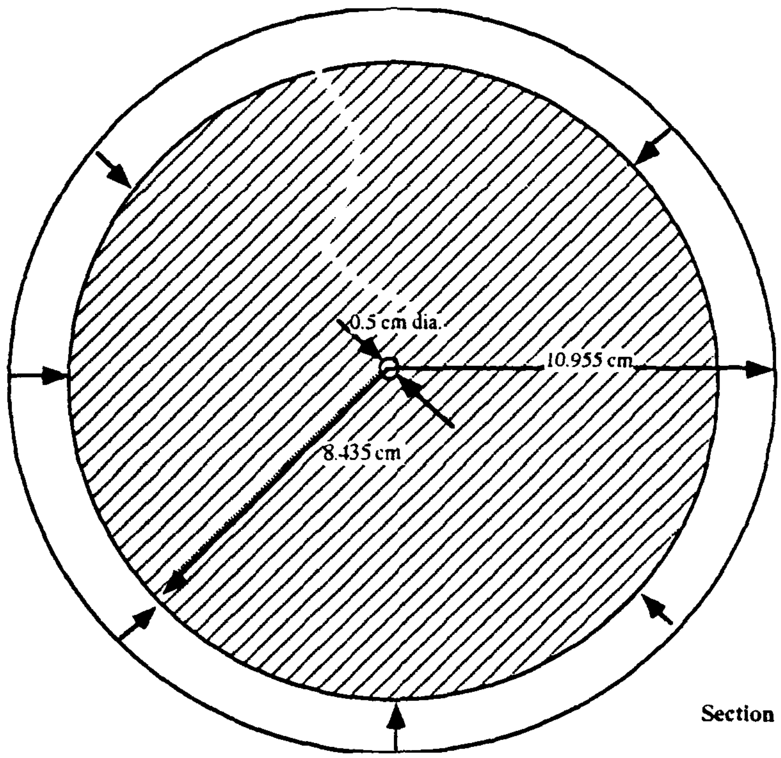


Figure A-4. Diagram of a cut through section C of figure A-1.

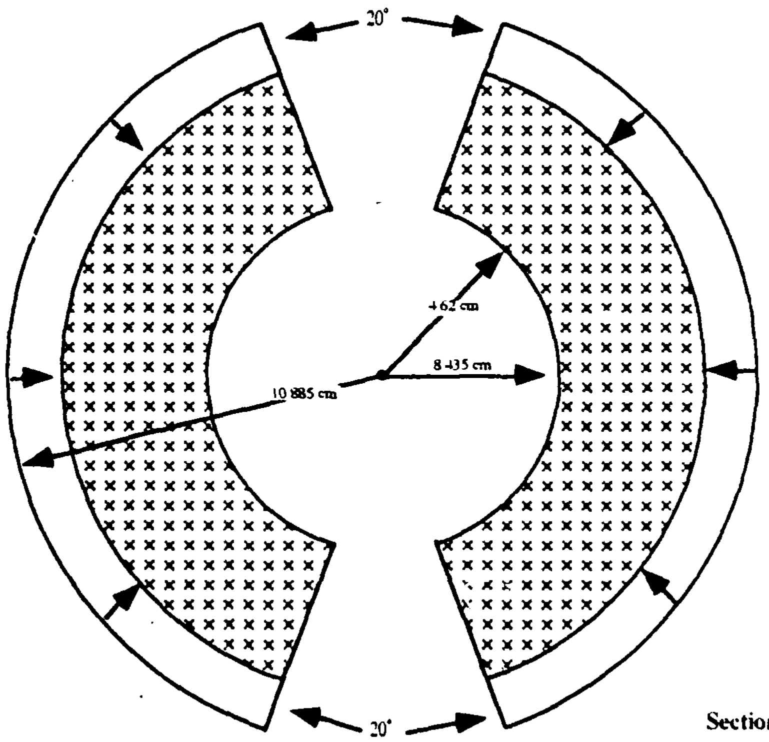


Figure A-5. Diagram of cut through section D of figure A-1.

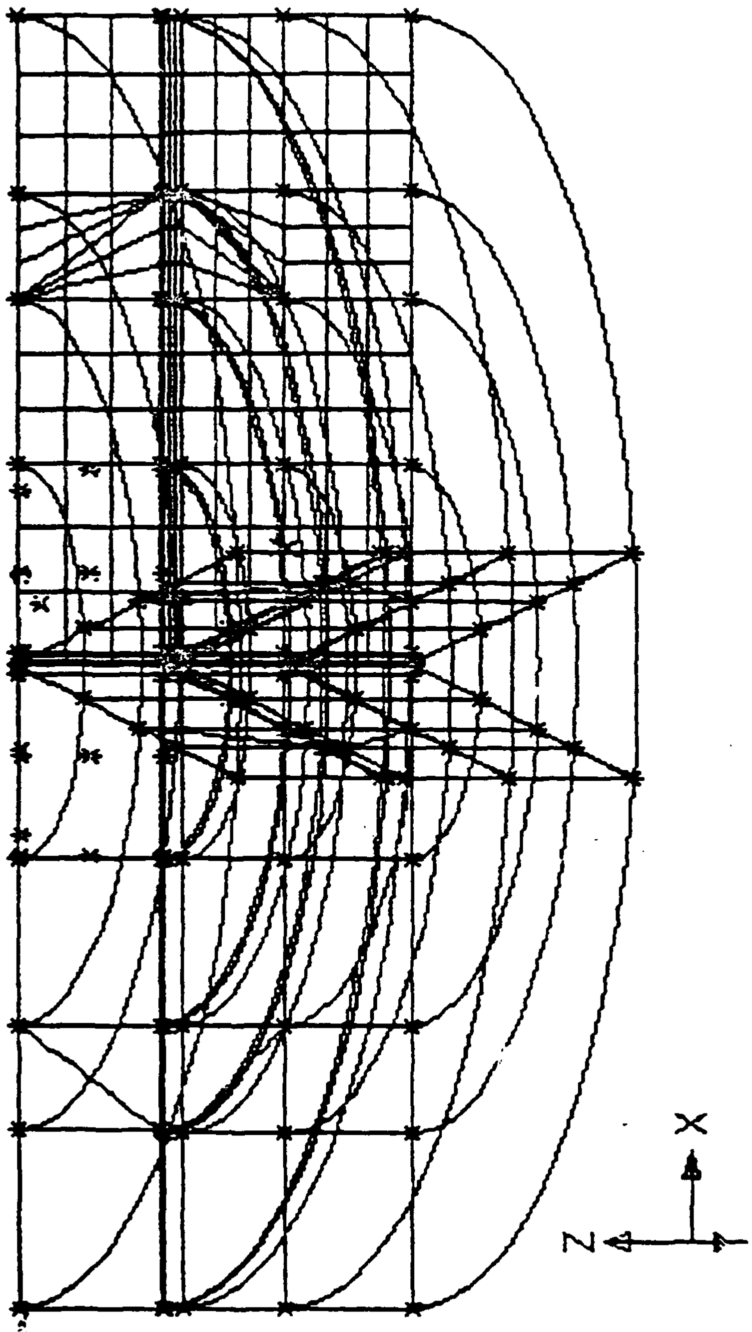


Figure A-6. Overall view of the structure modeled with one half the length and 180° around the circumference.

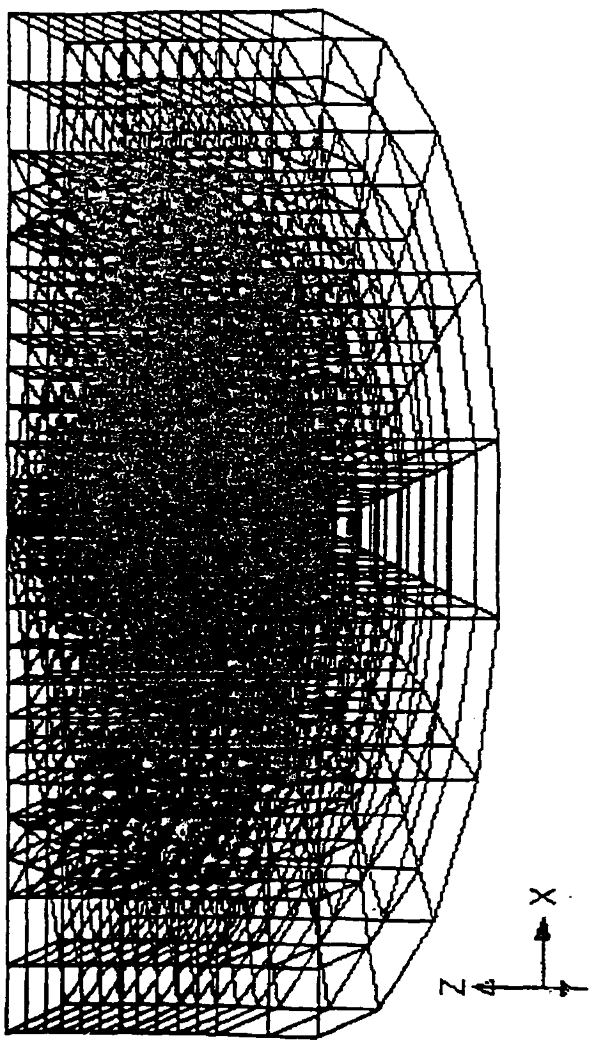


Figure A-7. Resulting three-dimensional finite element mesh of the structure as shown in Figure A-6. The structure is tilted 25° about the x-axis to make it easier to visualize.

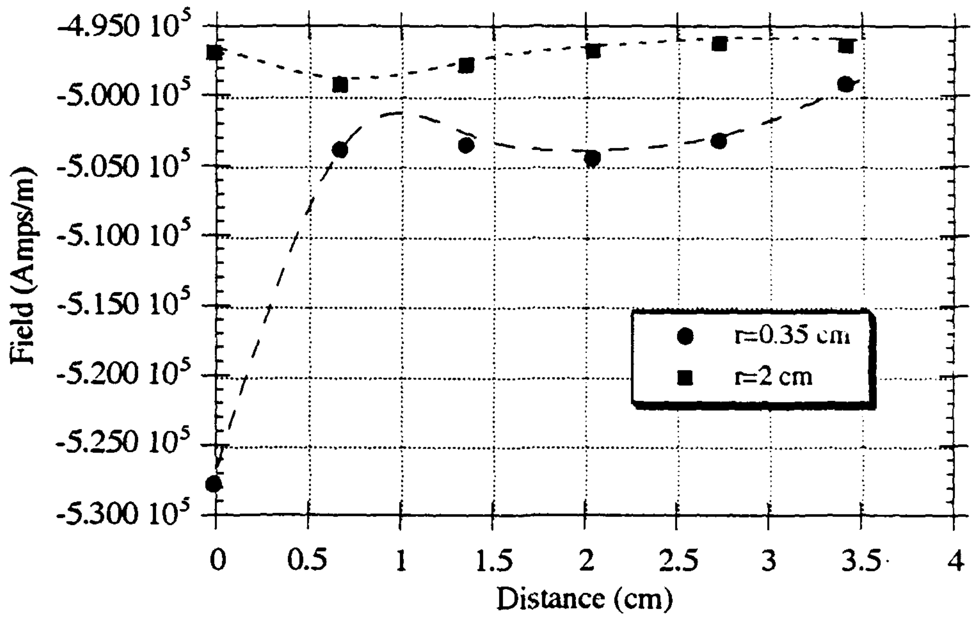


Figure A-8. $H_Z$ versus distance along z axis, $\theta=45°$.

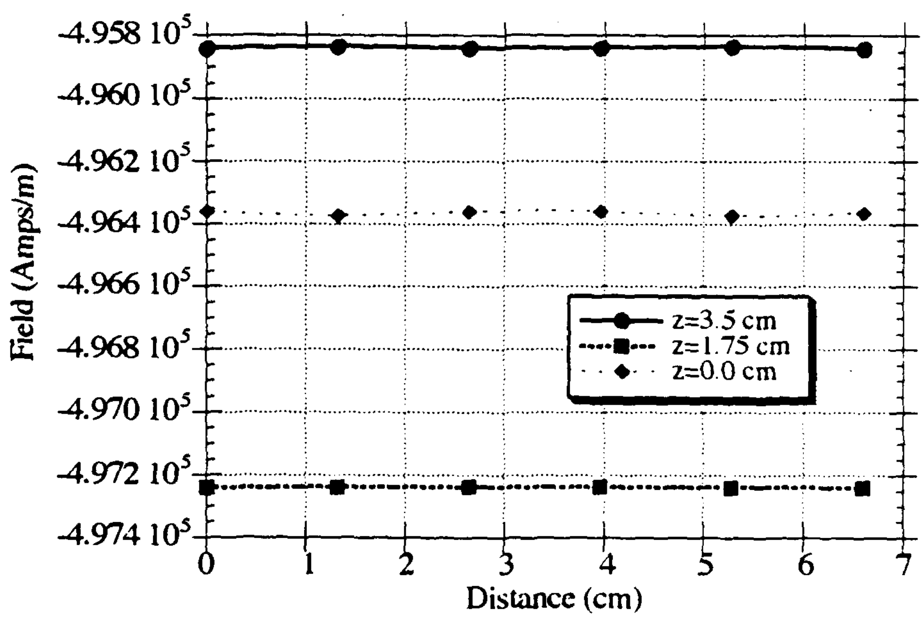


Figure A-9. $H_Z$ versus distance along arc from $\theta=0°$ to $\theta=180°$ at r=2.1 cm.

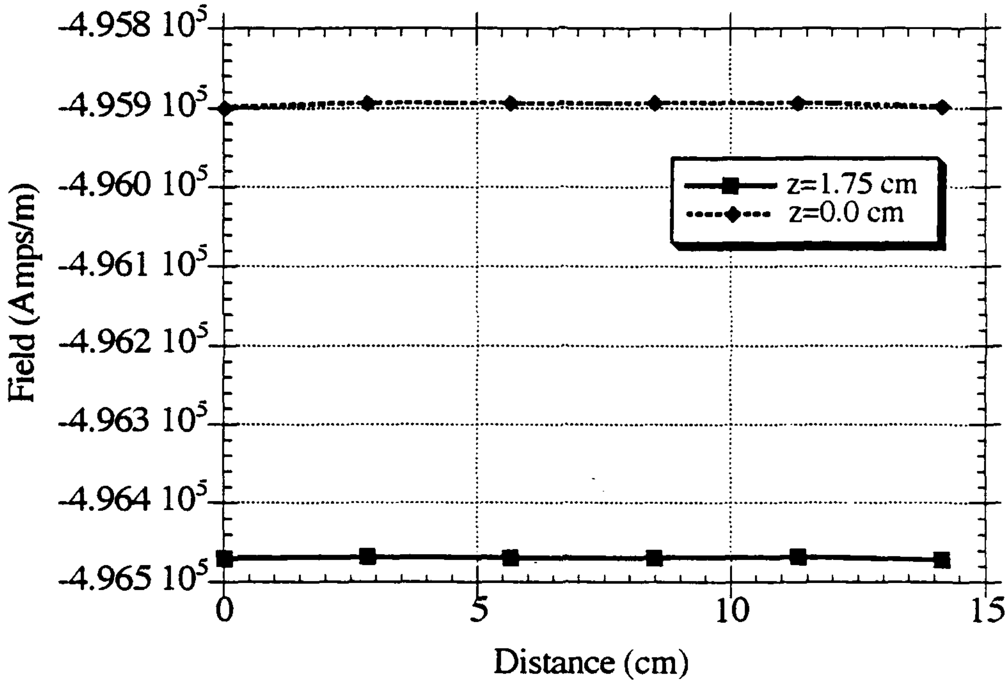


Figure A-10. $H_Z$ versus distance along arc from $\theta = 0°$ to $\theta = 180°$ at $r = 4.5$ cm.

ELECTRONICS TECHNOLOGY AND DEVICES LABORATORY
MANDATORY DISTRIBUTION LIST
CONTRACT OR IN-HOUSE TECHNICAL REPORTS

Defense Technical Information Center*
ATTN: DTIC-FDAC
Cameron Station (Bldg 5)
Alexandria, VA 22304-6145

(*Note: Two copies for DTIC will be sent from STINFO Office.)

Director
US Army Material Systems Analysis Actv
ATTN: DRXSY-MP
001 Aberdeen Proving Ground, MD 21005

Commander, AMC
ATTN: AMCDE-SC
5001 Eisenhower Ave.
001 Alexandria, VA 22333-0001

Commander, LABCOM
ATTN: AMSLC-CG, CD, CS (In turn)
2800 Powder Mill Road
001 Adelphi, Md 20783-1145

Commander, LABCOM
ATTN: AMSLC-CT
2800 Powder Mill Road
001 Adelphi, MD 20783-1145

Commander,
US Army Laboratory Command
Fort Monmouth, NJ 07703-5601
1 - SLCET-DD
2 - SLCET-DT (M. Howard)
1 - SLCET-DR-B
35 - Originating Office

Commander, CECOM
R&D Technical Library
Fort Monmouth, NJ 07703-5703
1 - ASQNC-ELC-IS-L-R (Tech Library)
3 - ASQNC-ELC-IS-L-R (STINFO)

Advisory Group on Electron Devices
ATTN: Documents
2011 Crystal Drive, Suite 307
002 Arlington, VA 22202

Director
Naval Research Laboratory
ATTN: CODE 2627
001 Washington, DC 20375-5000

Cdr, PM JTFUSION
ATTN: JTF
1500 Planning Research Drive
001 McLean, VA 22102

Rome Air Development Center
ATTN: Documents Library (TILD)
001 Griffiss AFB, NY 13441

Deputy for Science & Technology
Office, Asst Sec Army (R&D)
001 Washington, DC 20310

HQDA (DAMA-ARZ-D/Dr. F.D. Verderame)
001 Washington, DC 20310

Dir, Electronic Warfare/Reconnaissance
Surveillance and Target Acquisition Ctr
ATTN: AMSEL-EW-D
001 Fort Monmouth, NJ 07703-5206

Dir, Reconnaissance Surveillance and
Target Acquisition Systems Directorate
ATTN: AMSEL-EW-DR
001 Fort Monmouth, NJ 07703-5206

Cdr, Marine Corps Liaison Office
ATTN: AMSEL-LN-MC
001 Fort Monmouth, NJ 07703-5033

Dir, US Army Signals Warfare Ctr
ATTN: AMSEL-SW-OS
Vint Hill Farms Station
001 Warrenton, VA 22186-5100

Dir, Night Vision & Electro-Optics Ctr
CECOM
ATTN: AMSEL-NV-D
001 Fort Belvoir, VA 22060-5677

Cdr, Atmospheric Sciences Lab
LABCOM
ATTN: SLCAS-SY-S
001 White Sands Missile Range, NM 88002

Cdr, Harry Diamond Laboratories
ATTN: SLCHD-CO, TD (In turn)
2800 Powder Mill Road
001 Adelphi, MD 20783-1145